Data assimilation of radar reflectivity volumes in a LETKF scheme

Thomas Gastaldo[1,2], Virginia Poli[1], Chiara Marsigli[1], Pier Paolo Alberoni[1], and Tiziana Paccagnella[1]

[1]Arpae Emilia-Romagna Hydro-Meteo-Climate Service - Bologna, Italy
[2]University of Bologna - Bologna, Italy

Correspondence to: Thomas Gastaldo (thomas.gastaldo2@unibo.it)

Abstract. Quantitative precipitation forecast (QPF) is still a challenge for numerical weather prediction (NWP), despite the continuous improvement of models and data assimilation systems. In this regard, the assimilation of radar reflectivity volumes should be beneficial, since the accuracy of analysis is the element that most affects short-term QPFs. Up to now, very few attempts have been made to assimilate these observations in an operational set-up, due to the large amount of computational

5   resources needed and to several open issues, like the arise of imbalances in the analyses and the estimation of the observational error. In this work, it is evaluated the impact of the assimilation of radar reflectivity volumes employing a Local Ensemble Transform Kalman Filter (LETKF), implemented for the convection permitting model of the COnsortium for Small-scale Modelling (COSMO). A 4 days test case on February 2017 is considered and QPF is evaluated in terms of the SAL technique, an object-based method which allows to evaluate structure, amplitude and location of precipitation fields Results obtained

10 assimilating radar reflectivity volumes are compared to those of the operational system of the Hydro-Meteo-Climate Service of the Emilia-Romagna region (Arpae-SIMC), in which only conventional data are employed. Furthermore, some sensitivity tests are performed to evaluate the impact of the additive inflation, of the lenght of assimilation windows and of the reflectivity observational error. Finally, balance issues are assessed in terms of kinetic energy spectra and providing some examples of how these affect prognostic fields.

15 *Copyright statement.* TEXT

1   Introduction

Numerical weather prediction (NWP) models are widely used in meteorological centres to produce forecasts of the state of the atmosphere. In particular, they play a key role in the forecast of precipitation (Cuo et al., 2011), which arouses a great interest due to the many applications in which it is involved, like the issue of severe weather warnings or for decision making in several

20 branches of agriculture, industry and transportation. Therefore, an accurate quantitative precipitation forecast (QPF) is of great value for society and economic activities.

In recent years, the increase of available computing resources has allowed to increment NWP model resolution and to improve the accuracy of parametrization schemes (Clark et al., 2016). Despite that, QPF is still a challenge since it is affected by uncertainties in timing, location and intensity (Cuo et al., 2011; Röpnack et al., 2013). These errors arise partly from the

Nonlinear Processes
in Geophysics

Open Access

EGU

Discussions

chaotic behaviour of the atmosphere and from shortcomings in the model physics (Berner et al., 2015), but the main factor which affects the quality of QPF, especially in the short range (3-12 hours), is the accuracy of initial conditions (Dixon et al., 2009; Clark et al., 2016).

The initial condition (analysis) is generally produced by a data assimilation procedure which combines model state (background or first guess) and observations to provide the best estimate of the actual state of the atmosphere at a given time. In the last decades, different assimilation schemes have been proposed and implemented operationally in meteorological centres around the world. They can be divided in two families: those based on a variational approach, like three-dimensional variational data assimilation (3D-Var: Courtier et al., 1998) and four-dimensional variational data assimilation (4D-Var: Buehner et al., 2010b) and those based on the ensemble Kalman filter (EnKF: Evensen, 1994; Houtekamer and Mitchell, 1998). At the convective scale, EnKF methods seem to be preferable to variational schemes. In fact, they determine explicitly the background error covariance, which is highly flow-dependent at the convective scale. Furthermore, in a variational scheme is not straightforward to update any variable of a NWP model since an explicit linear and adjoint relation to the control vector of prognostic variables is needed. These problems are partly addressed by employing hybrid EnKF-Variational techniques (like Wang et al., 2008; Gustafsson and Bojarova, 2014) but these approaches have mostly been applied to larger scale NWP. Several variants of EnKF have been suggested (for a survey refer to Meng and Zhang, 2011) and one of the most popular is the local ensemble transform Kalman filter (LETKF), proposed by Hunt et al. (2007). It is used operationally in several meteorological centres like at COMET (Bonavita et al., 2010), at MeteoSwiss employing the version of the scheme developed for the COSMO consortium (Schraff et al., 2016) and for research purposes at the Japan Meteorological Agency (JMA; Miyoshi et al., 2010) and at the European Centre of Medium-Range Weather Forecasts (ECMWF; Hamrud et al., 2015)

The quality of the analysis is not determined only by the data assimilation scheme employed, but also by the quality and amount of observations that can be assimilated. With this aim, the assimilation of radar observations can be very beneficial, since they are highly dense in space (both horizontally and vertically) and in time. Up to now, several attempts have been made to improve the quality of analyses and subsequently the accuracy of QPFs by assimilating rainfall data estimated from radar reflectivity observations (Jones and Macpherson, 2006; Leuenberger and Rossa, 2007; Sokol, 2009; Davolio et al., 2017). Conversely, only recently EnKF techniques have been employed to directly assimilate reflectivity volumes in a convection permitting model (Bick et al., 2016) with some promising results. However, many issues affect the assimilation of reflectivity volumes at high spatial resolution and several aspects need to be further investigated.

First of all, the length of the assimilation window, which is one of the key aspects of any data assimilation system, has to be examined. In EnKF methods, a short window would be desirable to avoid that dynamical features leave the area where computed localized increments are significant (Buehner et al., 2010a). On the other hand, a too short window would lead to an increase of imbalances in the analysis, since the model has no the time to filter spurious gravity waves, introduced at each initialization, throughout the forecast step of the assimilation cycle. When reflectivity volumes are assimilated, the window length becomes even more crucial. In order to exploit the high temporal frequency of these data, which is essential to properly characterize fast developing and moving precipitation systems, it seems reasonable to employ short windows to assimilate, in each cycle, only observations collected very close to the analysis time. Furthermore, the choice of a short window is encouraged

by the use of a severe spatial localization, which has to be employed since small scales features are observed (Houtekamer and Zhang, 2016). Conversely, the big amount of radar observations enhances the instability issue and, therefore, the instability generated in the model by each initialisation should be checked and kept under control.

Another important issue is how to determine the observational error for radar reflectivities. As for any other observation, this

5 is influenced by three different sources: instrumental errors, representativity errors and observation operator errors. Since none of these is known, the choice of its value is not straightforward and can be estimated only in a statistical sense. Considering the amount of radar data, a correct estimation of the observational error is crucial, since even a small departure from the correct value can have a large impact on the quality of the analyses. Finally, it should be taken into account that the use of the radar data is highly dependent on the observation operator adopted and its biases should also be studied and ideally removed.

10 At Arpae-SIMC, the Hydro-Meteo-Climate Service of the Emilia-Romagna region, in Italy, a LETKF scheme is used to provide the initial conditions to the convection-permitting components of the operational modeling chain, consisting of one deterministic run and of one ensemble system both at 2.2 km of horizontal resolution. The purpose of this paper is to present the first results obtained by assimilating in this scheme the reflectivity volumes of the Italian radar network. In particular, it is studied the sensitivity of the obtained analysis to two important characteristics of the assimilation cycle: the length of each

15 cycle and the observational error attributed to the radar reflectivities.

This paper is organised as follows. In section 2, the model and the data assimilation system employed are described, as well as the observations employed and the set-up of the experiments performed. Furthermore, the verification method is explained. In section 3 results are shown and discussed. In section 4 some conclusions are drawn.

2   Data, model and methodology

20 ### 2.1   The COSMO model

The COSMO model (Baldauf et al., 2011) is a non-hydrostatic limited-area model developed by the multi-national COnsortium for Small-scale Modelling (COSMO) and it is designed for both operational NWP and several research applications. It is based on the primitive equations describing compressible flows in a moist atmosphere and the continuity equation is replaced by a prognostic equation for the pressure perturbation (deviation from a reference state). The prognostic variables involved in

25 these equations are the three dimensional wind vector, temperature, pressure perturbation, turbulent kinetic energy (TKE) and specific amount of water vapour, cloud water, cloud ice, rain, snow and graupel.

In the present study, the COSMO model is run at 2.2 km horizontal resolution over a domain covering Italy and part of the neighbouring countries (Figure 1) and employing 65 terrain-following hybrid layers.

Regarding set-up and parametrizations, deep convection is resolved explicitly while the shallow convection is parametrized

30 following the non-precipitating part of Tiedtke scheme (Tiedtke, 1989). Cloud formation and decay is controlled by a Lin-type one moment bulk microphysics scheme which includes all the prognostic microphysical species (Lin et al., 1983; Seifert and Beheng, 2001). The turbulent parametrization is based on a TKE equation with a closure at level 2.5, according to Raschendor-fer (2001). Radiative effects are described by the δ-two-stream radiation scheme of Ritter and Geleyn (1992) for short-wave
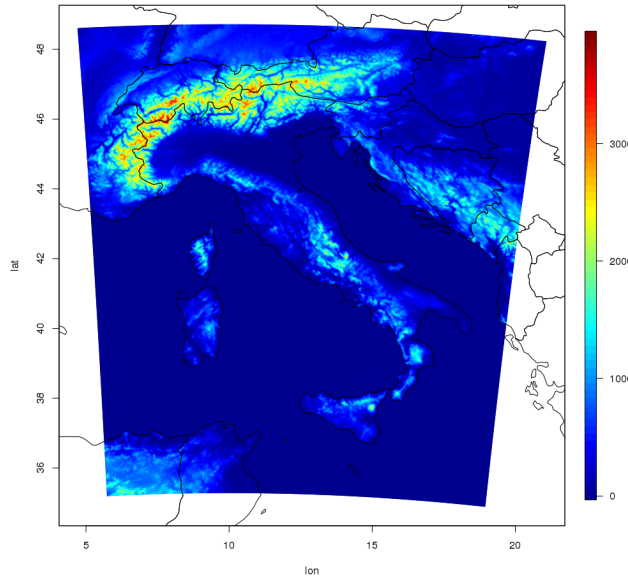
Figure 1. Integration domain and corresponding orography of the COSMO model employed in this study.

and long-wave fluxes. Finally, the lower boundary conditions at the ground are provided by the multi-layer soil model TERRA
(Doms et al., 2011).

2.2 The KENDA system

The KENDA system (Schraff et al., 2016) implements for the COSMO model the LETKF scheme described by Hunt et al.
(2007). In this implementation, the method is fully four dimensional, that is all observations collected during the assimilation
window contribute to determine the analysis and the related model equivalents are computed using the prognostic variables
at the proper observation time. The limited size of the ensemble, combined to the assumption of a perfect model made in the
LETKF scheme, leads to an underestimation of the background and analysis variances (e.g. Anderson, 2009) and, as a conse-
quence, the quality of analyses is negatively affected. To address this issue, KENDA provides some techniques to enlarge the
spread of the ensemble (for a complete description of each of them refer to Schraff et al., 2016). Here, multiplicative covariance
inflation (Anderson and Anderson, 1999) and the relaxation to prior perturbation (RTPP; Zhang et al., 2004) are employed.
The former consists in inflating the analysis error covariance by a factor ρ greater than one which is estimated following
Houtekamer et al. (2005). The latter lies on the relaxation of the analysis ensemble perturbations towards the background
ensemble perturbations by replacing at each grid point the analysis perturbation matrix in ensemble space $\mathbf{W}^a$ by

$$(1-\alpha_p)\mathbf{W}^a + \alpha_p\mathbf{I} \tag{1}$$

where $\mathbf{I}$ is the identity matrix and $\alpha_p = 0.75$ (see also Harnisch and Keil, 2015). Another approach provided by KENDA to
account for model error is the additive inflation. The basic idea is to add random noise with mean $\mathbf{0}$ and covariance $\mathbf{Q}$ to the

Figure 2. Domain covered by the composite of the Italian radar network.

analysis ensemble members, where $\mathbf{Q}$ is the model error covariance matrix (Houtekamer and Mitchell, 2005). Since $\mathbf{Q}$ is not known, it is assumed to be proportion (by a factor smaller than 1) to a static background error covariance $\mathbf{B}$ (Mitchell and Houtekamer, 2000). Additive inflation is used together with multiplicative inflation and to RTPP only in one experiment, using a climatological $\mathbf{B}$-matrix from the 3D-VAR of the ICON model (Zängl et al., 2015).

2.3 Assimilated data

KENDA allows the assimilation of both conventional and non conventional observations.

Conventional observations assimilated in this work include aircraft measurements (AMDAR) of temperature and horizontal wind, surface station measurements (SYNOP) of 10 m horizontal wind, 2 m temperature, 2 m relative humidity and surface pressure, radiosonde data (TEMP) of temperature, horizontal wind and humidity.

Fields of surface rainfall rate (SRI) are also assimilated in each member of the assimilation ensemble using a Latent Heat Nudging Scheme (LHN; Stephan et al., 2008). SRI data come from the composite of Italian radar network and are distributed by the National Department of Civil Protection and cover the area of Figure 2.

These data have a temporal resolution of 10 minutes and a spatial resolution of 1 km, but before the assimilation they are interpolated at the model resolution. The composite is obtained as a weighted average of surface rain rates from single stations, where weights are represented by quality. Data coming from each radar station undergo:) a quality control that removes data with low quality depending in particular on the distance from the radar station itself. These fields are assimilated through the Latent Heat Nudging scheme, based on the fact that the latent heat, integrated along the vertical column, is approximately proportional to the precipitation observed. It acts in rescaling temperature profiles with an adjustment of the humidity field
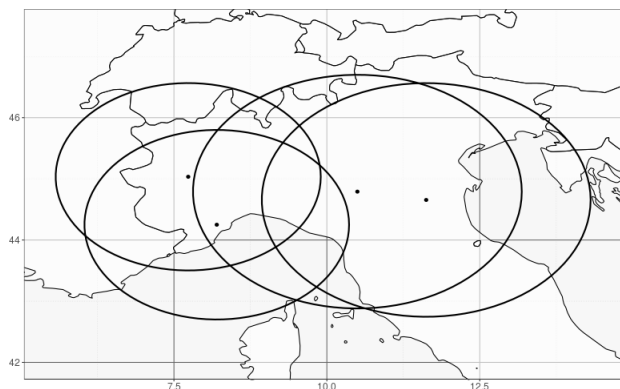
Figure 3. Domain covered by radar systems used in this study at their lowest elevation beam angle

according to the ratio between observed and modelled rain rates. LHN is applied continuously during the integration of the model and it is able to capture the dynamical structure and the right rainfall amount of the storm in a perfect environment and it can be gainfully used also in complex terrain (Leuenberger and Rossa, 2004; Leuenberger and Rossa, 2007). In the KENDA framework this allows to have the model first guess closer to the observed atmospheric state, improving the analysis quality.

5   With regards to non conventional observation, KENDA allows also the assimilation of radar reflectivity volumes and radial winds. Radar data are assimilated through the Efficient Modular VOlume RADar Operator (EMVORADO) expressly designed for the COSMO model. It simulates the radar reflectivity factor and radial velocities processing the COSMO model fields one radar system at a time. Operator characteristics, resolution and the management of no-precipitation information are described in (Bick et al., 2016).

10   In the present work, radar reflectivities volumes are assimilated, but only on Northern Italy. Radar reflectivity volumes come from four different radar stations: Bric Della Croce (Piedmont Region), Settepani (Liguria Region), Gattatico and San Pietro Capofiume (Emilia-Romagna Region). Due to the complex orography of the considered area, radar are placed at very different altitudes and have different acquisition strategies. Observations are acquired every 10 minutes for Bric Della Croce radar, every 5 minutes for Settepani radar, every 15 minutes for San Pietro Capofiume radar and every 15 minutes starting from minutes 05

15   and 10 of each hour for Gattatico radar. At lowest beam elevation angle the covered domain is presented in Figure 3.

Raw reflectivities are pre-processed to eliminate non meteorological echoes, in particular, to eliminate the clutter signal that would affect the analysis retrieval introducing spurious observations. Data have a range resolution of 1 km, while the azimuthal resolution is 1 degree for Bric Della Croce and Settepani and 0.9 degree for San Pietro Capofiume and Gattatico. Due to the fact that volumes from single radars undergo different pre-processing, it is not possible to define a homogeneous quality criterion.

20   For this reason all data in the volume, that are not rejected from pre-processing step, are supposed to have the same quality and are used into the assimilation cycle.

The high temporal and spatial density of observations is precious to estimate the initial state of numerical weather forecast. This allows to gather a lot of information on the real state of the atmosphere, but it determines an increase in analysis compu-

6

tational cost, in data transfer time and in memory disk occupation. Moreover, a spatial and/or temporal high density violates the assumption made in the most part of assimilation schemes: the non-correlation of observational errors. To reduce the total amount of data and to extract essential content of information, the superobbing technique is chosen. In this way, reflectivities over a defined area are combined through a weighted mean into one single observation representative of the desired greater

5 spatial scale. As in Bick et al. (2016), the horizontal resolution chosen in this work for the superobbing is equal to 10 km. Furthermore, before performing superobbing, a threshold of 5 dBZ is applied to observed and simulated fields in order to avoid that large innovations associated to non-precipitating signals would lead to large analysis increments without physical relevance.

To evaluate the observational error, a diagnostic based on statistical averages of observations-minus-background and observations-

10 minus-analysis residuals, as described in Desroziers et al. (2005), is used. The estimated value is, on average along the vertical, 5 dBZ, as found also by Tong and Xue (2005).

2.4   Experimental set-up

The KENDA system is implemented operationally at Arpae using an ensemble of 20 members plus a deterministic run, which is obtained by applying the Kalman gain matrix for the ensemble mean to the innovations of the deterministic run itself.

15 In principle, ensemble mean analyses can be deployed to initialize the deterministic forecasts, but this would lead to some inaccuracies since the mean of a non-Gaussian ensemble is generally not in balance (Schraff et al., 2016). For this reason the deterministic branch is added to the system, which differs from the ensemble ones only due to boundary conditions. The ensemble members use lateral boundary conditions provided each 3 hours at a 10 km horizontal resolution by the ensemble of the data assimilation system of the Centro Operativo per la Meteorologia (COMet), based on a LETKF scheme (Bonavita

20 et al., 2010). The deterministic run employs hourly boundary conditions provided by a 5 km version of COSMO run at Arpae (COSMO-5M) which domain covers a large part of the Mediterranean basin ans surrounding countries.

In the operational set-up, the COSMO model configuration described in Section 2.1 is adopted for all the 21 members. At present, in the operational chain only conventional observations are assimilated and LHN is performed on each member of the ensemble. The KENDA analyses are used operationally to provide initial conditions to COSMO-2I, the 2.2 km determinstic

25 run initialized twice a day at 00 UTC and 12 UTC and to COSMO-2I EPS, an ensemble which is run every day at 00 UTC for a 48 hours forecast range. In this work, deterministic forecasts starting from the KENDA deterministic analysis are also performed, in order to evaluate the quality of the analysis also from its impact when used to initialise a forecast.

To evaluate the impact of the assimilation of reflectivity radar volumes, several experiments are performed employing different configurations. The complete list is provided in Table 1. In the control experiment, called *conv60*, the set-up of the

30 operational chain is replicated: conventional data are assimilated in KENDA in cycles of 60 minutes and the LHN is performed during the forecast step of each assimilation cycle. All the other experiments involve the assimilation of both conventional data and reflectivity volumes, in addition to LHN. In the *rad60* experiment, radar measurements are assimilated using a reflectivity observation error (*roe*) of 5 dBZ and a 60 minutes assimilation window is employed. A comparison with *conv60*, from which *rad60* differs only due to the inclusion of radar data in the KENDA system, allows an assessment of whether, under the same

conditions, the assimilation of reflectivity observations improves the quality of analyses. The same set-up of *rad60* is employed in the experiment *rad60_Bm*, but additive inflation is applied to increase the spread of the ensemble.

Trial	Window length [min]	Assimilated obs.	roe [dBZ]	Note
conv60	60	conv.	-	-
rad60	60	conv. + radar	5	-
rad60_Bm	60	conv. + radar	5	Additive inflation
rad30	30	conv. + radar	5	-
rad15	15	conv. + radar	5	-
rad60_lst15	60	conv. + radar	5	Use obs. in the last 15 min. of the window
rad60_roe10	60	conv. + radar	10	-
rad60_roe0.5	60	conv. + radar	0.5	-
rad15_roe10	15	conv. + radar	10	-
rad15_roe0.5	15	conv. + radar	0.5	-

Table 1. Experimental set-up of each trial including the length of the assimilation cycles, the type of observations assimilated, the reflectivity observation error (*roe)* associated to radar data and any additional feature.

In order to test the impact of assimilating only observations which are not too far from the analysis time, experiments on the duration of the assimilation windows are performed. This is tested by comparing *rad60* to experiments *rad30* and *rad15* which differ from *rad60* only for the length of the assimilation window, equal to 30 and 15 minutes respectively. An alternative way to assimilate only the most relevant observations is to select in each cycle a subset of data including the closest to the analysis time. In the experiment *rad60_lst15* an assimilation window of 60 minutes is employed but only the observations (both conventional and radar reflectivities) collected in the last 15 minutes of the cycle are taken into account.

Since the estimation of observation error is not straightforward and different techniques can be applied, it is worth to evaluate the sensitivity of the assimilation system to this parameter. In addition to the value of 5 dBZ employed in the previous experiments, two other values are selected: 10 dBZ or 0.5 dBZ. Both of them are tested employing a 60 minutes assimilation window (*rad60_roe10* and *rad60_roe0.5*) and using 15 minutes cycles (*rad15_roe10* and *rad15_roe0.5*).

The experiments described above are carried out over a period of almost 4 days from 3 February 2017 at 06 UTC to 7 February 2017 at 00 UTC. During 3 and 4 February, middle tropospheric circulation over Northern and Central Italy was dominated by southwesterly divergent flows associated with the passage of some precipitating systems. In 5 February a trough moved from France to Italy and this caused the formation of new precipitations in Northern Italy. During 6 February the trough moved slowly from Central Italy to the southern part of the country and precipitations weaken gradually. For each experiment, a set of 5 forecasts up to 48 hours is initialized using the analyses generated during the assimilation procedure. Initialization times employed are 04 February at 00 and 12 UTC, 5 February at 00 and 12 UTC and 6 February at 00.

2.5 Verification

The performance of each experiment described in the previous section is assessed in terms of QPF employing two methods. The first consists of comparing the area-average values of 3-hourly precipitation: average precipitation forecasted by the model over an area is compared against the average precipitation observed by raingauges (nearly 1500 stations) over the same area. In order to have comparable samples, precipitation forecasted by the model is first interpolated on station location (by selecting the value at the nearest grid point). The second method employs the SAL metrics (Wernli et al., 2008), an object based verification score which allows to overcome the limitations of traditional scores for convection-permitting models, like the double-penalty problem (Rossa et al., 2008). The detection of individual objects in the accumulated precipitation fields is achieved by considering continuous areas of grid points exceeding a selected threshold. Comparing objects from observed and forecast fields, SAL provides information about the structure S, the amplitude A and the location L errors of QPF. A perfect match between forecast and observations would lead to $S = A = L = 0$; the more values differ from 0, the greater the disagreement between model and observations. More in detail, a too sharp/flat (broad/small) structure of forecast precipitation compared to observations is associated to positive (negative) values of S; an overestimation (underestimation) of average rainfall over the domain is associated to positive (negative) values of A; a misplacement of precipitation nuclei leads to positive values of L. Note that L can range between 0 and 2, while S and A between -2 and 2.

Observations employed to perform SAL consist in 3-hourly accumulated precipitation estimated from the Italian radar network and corrected using rain-gauges data. The radar estimates are derived from the SRI product which is assimilated in each run with the LHN method, therefore they are not independent observations. Nevertheless, the assimilation takes place in all experiments, making possible the use of this product for the evaluation of their relative performances. The radar-raingauges adjustment, adapted for a radar composite, derives from the method described in Koinstinen and Puhakka (1981). The original method comprises two terms: a range dependency adjustment and a spatial varying adjustment. In our case, only the second term is taken into account due to the fact that, in overlapping areas of the composite, rainfall estimation is obtained combining data from different radars and, therefore, the original information on the range distance from the radar is lost. The correction is based on a weighted mean of the ratio between rain gauges and estimated radar rainfall amount calculated over the station locations. Weights are a function of the distance of the grid point from the station and of a filtering parameter calculated as the mean spacing between 5 observations. Then a smoothing factor is applied to the correction.

The verification area is shown in Figure 4.

This choice is made to assess the impact of the assimilation of radar reflectivity volumes in the region where these data are actually observed. Furthermore, regarding SAL, in Wernli et al. (2009) it is recommended to use a domain not larger than $500 \times 500 \text{ km}^2$ since, otherwise, the domain may include different meteorological systems making the interpretation of results problematic.
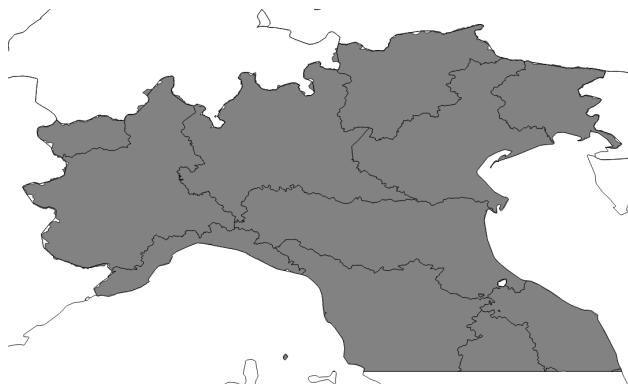
Nonlinear Processes
in Geophysics

Discussions

Open Access

EGU

Figure 4. Verification domain over Northern Italy is highlighted in dark grey

3 Results

3.1 Impact of assimilating the radar reflectivities

A preliminary assessment of the impact of assimilating radar reflectivity volumes with the KENDA system is provided by comparing *conv60*, in which only conventional observations are employed, and *rad60*, in which radar reflectivity data are added. It is reminded that LHN of radar precipitation estimates is also applied in both experiments. Area-average 3-hourly precipitation forecasted during the assimilation procedure is displayed in Figure 5 for three experiments, employing precipitation recorded by rain-gauges (black line) as independent observation. Since the duration of each assimilation cycle is 1 hour, the precipitation forecasted by the model during each hour is accumulated in order to obtain the 3-hourly precipitation. Overall, the correspondence of *rad60* (green, which will be used from here onwards to identify uniquely this experiment) to observations is equal or better than that of *conv60* (red). In some cases the improvement is particularly relevant, like at 21 UTC on 3 February and at 15 UTC on 4 February. Only at 00 UTC on 4 February the performance of *conv60* is clearly better than that of *rad60*.

The same set-up of *rad60* is used in the experiment *rad60_Bm*, but with the addition of additive inflation to enlarge the ensemble spread. Mean precipitation during the assimilation cycles (blue line in Figure 5) differs from that of *rad60* but, since slight improvements at some instants are compensated by slight deteriorations at others, the overall impact of the use of additive inflation seems to be neutral.

For the five forecasts initialized from the analyses of each experiments, the precipitation is verified using SAL and employing a 1 mm threshold to identify rainfall objects. In Figure 6 the average of the absolute value of each component of SAL is plotted as a function of lead time. Although forecasts are up to 48 hours, the verification is shown only for the first 24 hours, since after this lead time scores of the different experiments become very close. The average is computed considering only cases in which the observed rainfall field consists of at least 1000 grid points (3 events at lead time +6h, 4 otherwise). Using the absolute value of the components of SAL, only the magnitude of the error is considered, loosing the information on the type of error (e.g., for *A*, an overestimation of forecast precipitation cannot be distinguished from an underestimation). This choice
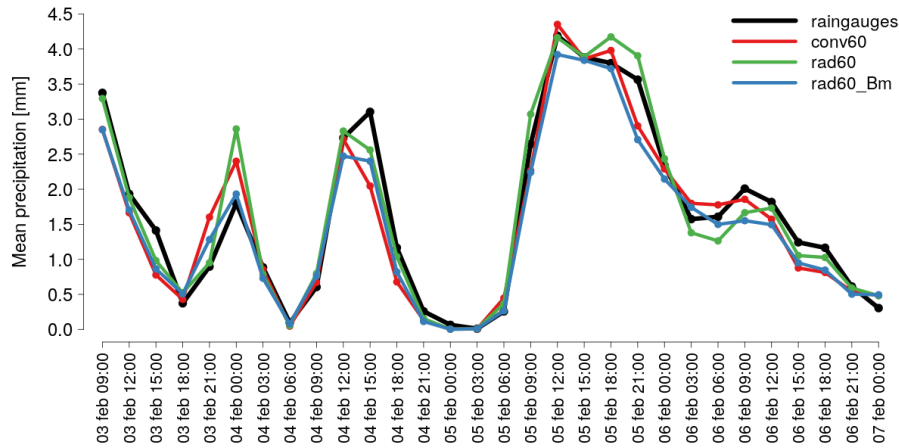
Figure 5. Area-average 3h precipitation for rain-gauges (black) in the verification area shown in Figure 4 and at the corresponding model forecast relative to experiments *conv60* (red), *rad60* (green) and *rad60_Bm* (blue), during the assimilation procedure.

slightly limits the potential of SAL but provides an intuitive picture of the overall performance of each experiments (a similar approach is employed by Davolio et al., 2017). Differences between forecasts initialized from *conv60* and from *rad60* analyses are very small. Overall, the location of precipitations (*L* component) of *rad60* forecasts is only slightly improved compared to *conv60* forecasts. The amplitude error *A* is generally smaller in the first 12 hours, but from 15h onward the *conv60* forecasts

5   outperform the *rad60* forecasts. Regarding the structure component *S*, smaller errors for *rad60* forecasts at some lead times are counterbalanced by smaller errors for *conv60* at other lead times, in a non coherent way. Therefore, even if the use of analyses obtained by assimilating reflectivity volumes affects the structure of forecast precipitation, it is not possible to state if it is improved or deteriorated.

    The addition of the additive inflation (*rad60_Bm*, blue bars) does not show a positive impact. At lead time +6h a clear

10 worsening of each of the 3 components of SAL can be noticed.

3.2   Impact of the length of the assimilation cycles

To obtain some insights about this topic, assimilation cycles of 15 and 30 minutes (respectively *rad15* and *rad30*) are tested and the results are compared with those obtained with the 60 minutes window (*rad60*). In the same way described in the previous subsection, SAL verification is computed and averaged over the 5 forecasts initialized from the analyses of each trial. Results

15 are shown in Figure 7 where the green bars are associated to *rad60* while red and orange to *rad15* and *rad30* respectively. Regarding the location error, during the first 6 hours of forecast the performance of *rad15* is similar to that of *rad30* and both are worse than *rad60*. Afterwards, the 3 experiments provides a very similar performance. In terms of structure and amplitude components, the differences among the 3 different window lengths are generally small and non coherent over the 24 hours of forecast.
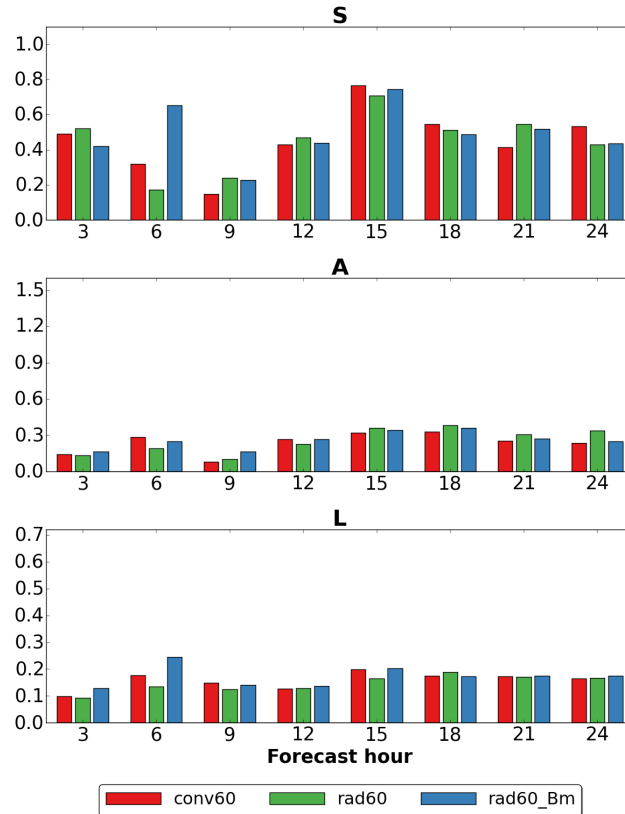
Figure 6. Average of the absolute value of each component of SAL over the 5 forecasts initialized from *conv60* (red), *rad60* (green) and *rad60_Bm* (blue) analyses. Three-hourly precipitation is considered employing a threshold of 1mm. Cases in which the observed precipitation field consist of less than 1000 points are not taken into account in the average.

In a further test, conventional and radar observations are assimilated only if collected during the last 15 minutes of each assimilation cycle of 60 minutes (*rad60_lst15*). In this way, the total amount of assimilated data is reduced and the increments computed by the LETKF scheme should be more appropriate for computing the analysis, since the observations time is always very close to the analysis time. Actually, verification shown in Figure 7 (blue bars) does not point out an improvement of *rad60_lst15* if compared to *rad60*. In fact, except for a worsening in the *S* component at forecast time +3h and +6h, performance of both experiments is very similar. Therefore, the assimilation of data closer to analysis time does not improve the forecast quality.

In order to evaluate the instability issue, the kinetic energy (KE) spectra of the experiments is computed following the method described in Errico (1985). Curves displayed in Figure 8 are obtained as an average over the whole assimilation period (from 3 February at 06 UTC to 7 February at 00 UTC) of KE spectra computed each hour using analysis values of *u*, *v* and *w* over the whole domain. Kinetic energy spectra of *rad15* (red) and *rad60* (green) are almost overlapping, even at very small wavelength. Furthermore, both spectra have a $-5/3$ dependence on the wavenumber beyond a wavelength of 15-20 km, in agreement with
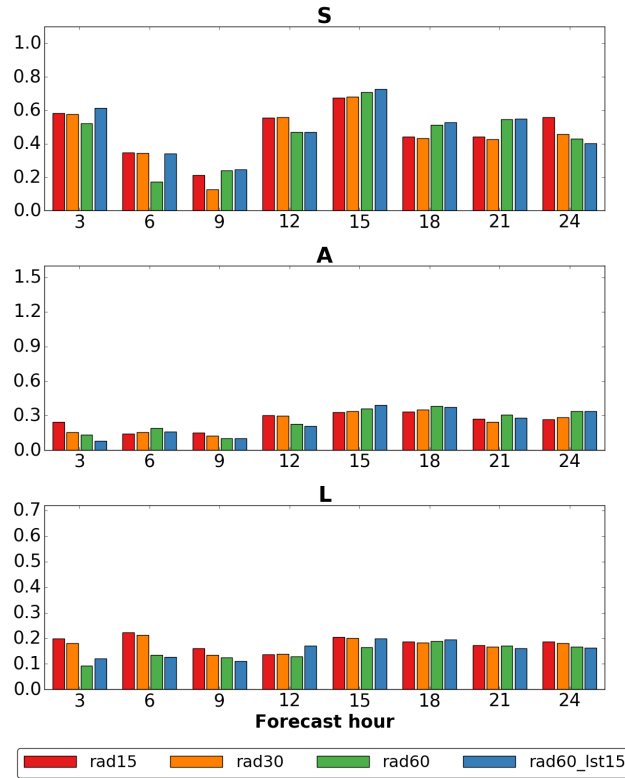
Figure 7. As in Figure 6 but considering experiments *rad15* (red), *rad30* (orange), *rad60* (green) and *rad60_lst15*) (blue).

observed spectra at the mesoscale (Nastrom and Gage, 1985). Same considerations apply also to KE spectra of *rad30* and to *rad60_lst15*, which are not shown.

As a conclusion, with the current set-up, the use of a sub-hourly window length does not introduce imbalances in the analysis. It is anyway observed a slightly worsening of the precipitation forecast, especially in terms of location of rainfall nuclei.

5 ### 3.3 Impact of changing the reflectivity observational error

A set of experiments is performed to investigate the impact of the reflectivity observation error in the assimilation scheme. In addition to the value of 5 dBZ employed so far, two other values of *roe* are tested: 10 dBZ and 0.5 dBZ. The former is employed by Bick et al. (2016) for the assimilation of reflectivity volumes from the German radar network using KENDA and COSMO and, therefore, should be reasonable also for the present study. The latter is a deliberately extreme value that may be chosen in

10 the case of a great confidence in the quality of radar observations. These two different values of *roe* are used in assimilation cycles of 60 minutes (*rad60_roe0.5* and *rad60_roe10*) and 15 minutes (*rad15_roe0.5* and *rad15_roe10*). Therefore, they can be compared with the experiments with our standard value of roe = 5dBZ, respectively *rad60* and *rad15*.
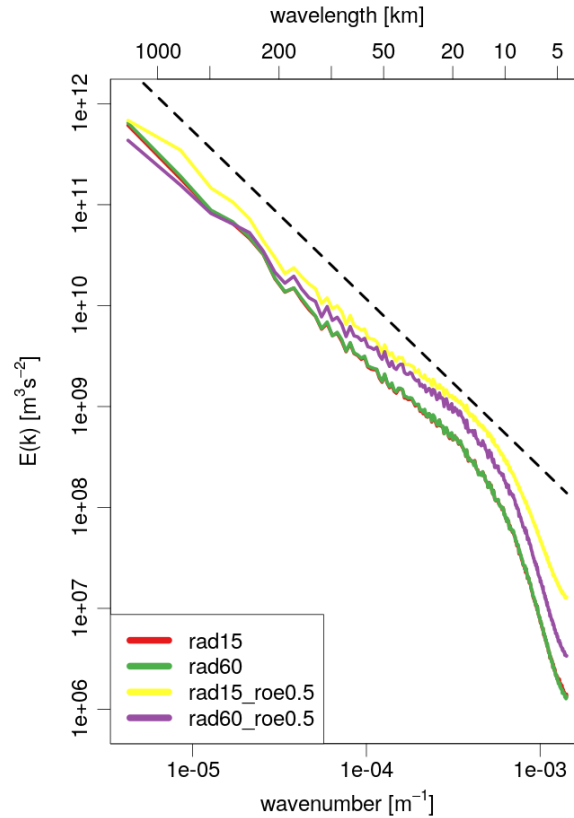
Figure 8. Kinetic energy (KE) spectra computed following the method described by Errico (1985). Each curve is obtained averaging KE spectra computed with a frequency of one hour during the assimilation procedure and employing analysis values of *u*, *v* and *w* over the whole model domain. The spectra are displayed for experiments *rad15* (red), *rad60* (green), *rad15_roe0.5* (yellow) and *rad60_roe0.5* (violet). The dashed black line represents a function with a dependence to the wavenumber equal to $-5/3$.

Verification of forecasts initialized from the analyses of these experiments is reported in Figure 9. Regarding the experiments with a 60 minutes assimilation cycle (left panel), the performance of *rad60_roe0.5* is clearly worse than that of *rad60*. In fact, up to the lead time of +15h, each component of SAL for the former (violet) is almost equal or greater than that of the latter (green) with the only exception for *S* at +3h. From +18h onwards, differences between the two become very small. On the other hand, the performance of *rad60_roe10* forecasts (orange) is very similar to that of *rad60* at any lead time, apart for the error in the structure of precipitation at +6h and +9h which is significantly greater for roe = 10dBZ. When considering assimilation cycles of 15 minutes (right panel in Figure 9), the worsening of forecast precipitation employing a roe = 0.5dBZ (yellow) compared to roe = 5dBZ (red) is further enhanced. In particular, precipitation in the first 12 hours is largely mis-placed and its total amount is widely different from observations. In this regard, the verification of individual forecasts (not shown here)
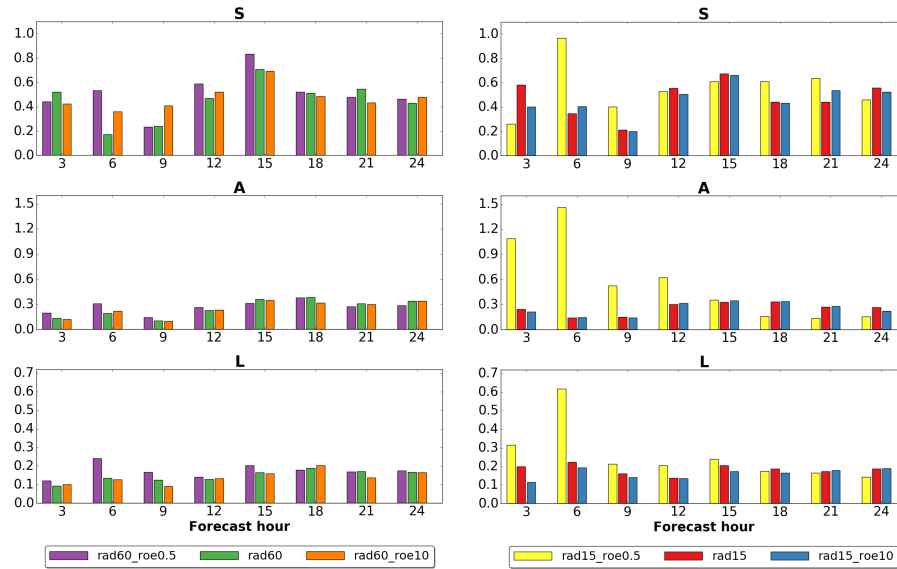
14

Figure 9. As in Figure 6 but considering, in the left panel, experiments *rad60_roe0.5* (violet), *rad60* (green) and *rad60_roe10* (orange) while, in the right panel, experiments *rad15_roe0.5* (yellow) *rad15* (red) and *rad15_roe0.5* (blue).

reveals that the large error in *A* component is due to a systematic underestimation of the average precipitation over the domain. Regarding *rad15_roe10* (blue), similarly to what observed for 60 minutes cycles, the use of roe = 10dBZ instead of 5 dBZ does not affect radically the quality of forecasts, even if a slight improvement in each component of SAL can be observed at +3h.

5   The overall poor quality of *rad15_roe0.5* forecasts is the direct consequence of the poor quality of the analyses from which they are initialized. As an example, in Figure 10 it is shown the mean sea level pressure (MSLP) and specific humidity at 850 hPa of *rad15_roe0.5* (right column) analysis on February 5 at 12 UTC and it is compared with the same quantities for the analysis of *rad60* (central column) and of the Integrated Forecasting System (IFS) of ECMWF (left column). Slight variations can be observed between IFS and *rad60* analyses and it seems reasonable that they may simply arise from differences between

10   models and assimilation systems. Conversely, *rad15_roe0.5* analysis exhibits a noticeable increase in MSLP and a decrease in specific humidity over Northern Italy. This is in agreement with the decrease in forecast precipitation previously described.

In the same way as described in Section 3.2, KE spectra are computed for *rad15_roe0.5* and *rad60_roe0.5* and displayed in Figure 8. In both cases, at the smallest wavelength the KE is significantly grater that that of *rad15* or *rad60* and this is particularly evident for *rad15_roe0.5*. This behaviour is indicative of the presence of some undesired noise at small scales

15   (Skamarock, 2004). Therefore, employing a value of *roe* equal to 0.5 dBZ, the assimilation system is not able to correctly remove small scale structures, especially when really short cycles are employed. Furthermore, the excess of energy associated to the highest wavenumber modes propagates to the larger scales and the slope of the curves at wavelengths greater than 15 km differs from -5/3.
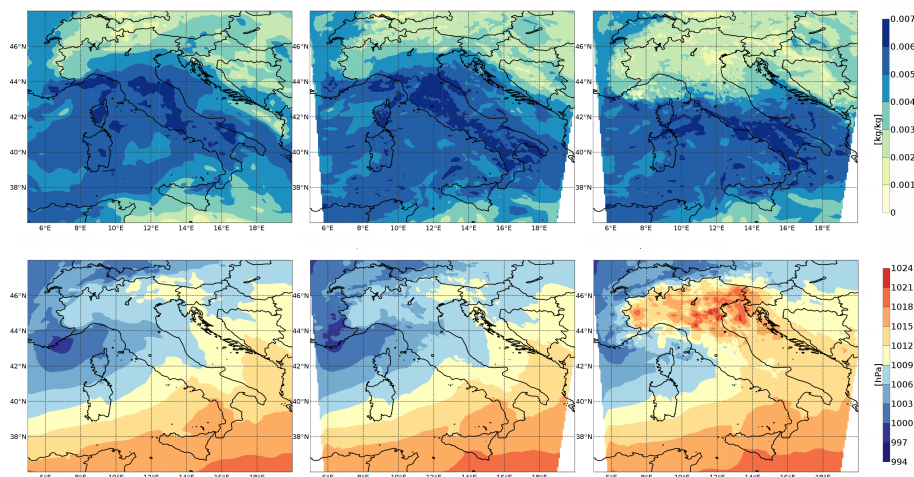
Figure 10. Mean sea level pressure (top) and specific humidity at 850 hPa analysis on February 5 at 12 UTC for IFS (left) *rad60* (middle) and *rad15_roe0.5* (right).

4 Conclusions

In the present work, the assimilation of reflectivity volumes in a high resolution model employing a LETKF scheme is evaluated. Assimilation of radar data is a challenging issue and most of the previous studies is devoted to the assimilation of rainfall estimation, while very few to the direct employment of reflectivity observations. Here, results in terms of QPF obtained

5 assimilating reflectivity volumes from 4 radars of the Italian network are shown and compared to those produced with the current operational assimilation system, in which only conventional data are employed. Furthermore, some sensitivity tests are performed to investigate the impact of some parameters which can substantially affect the quality of analyses.

The assimilation of radar reflectivity volumes with our selected set-up (*rad60*) only slightly improves QPF both during the assimilation procedure and for the subsequent forecasts, compared to the assimilation of only conventional data. This result

10 could be partly ascribed by the fact that radar data are already assimilated in the *conv60* experiment, in form of LHN of radar precipitation estimate. Even if the precipitation estimate is only a product derived by applying a complex algorithm to the volume of reflectivities, nevertheless its ingestion could influence the analysis so much that it is difficult to add benefit with the assimilation of reflectivities themselves. It has also been shown that, even if the spread of the ensemble is very small (not shown), its enlargement by employing additive inflation does not improve the performance, instead, it leads to a modest

15 worsening of the results. One possible reason for this behaviour can be the use of a climatological **B** matrix generated from the ICON model run at a very different resolution. This test should be repeated when a **B** matrix provided by the COSMO model over the Italian domain will be available.

For the case study considered in this work, the assimilation of data close to analysis time (at most collected 15 minutes before) does not improve the quality of forecast obtained when all observations collected in the whole assimilation window

20 are employed. Nevertheless, this results suggests that this configuration can be employed without evident downsides to reduce

the computational cost of the KENDA system. Further tests would be necessary to evaluate if the same conclusion arises when only observations at the analysis time are assimilated. Investigation of the instabilities generated with short assimilation cycles shows that the use of a sub-hourly window length does not introduce imbalances in the analysis, but it slightly worsens the forecast of precipitation, especially in terms of location of rainfall nuclei.

5   With regards to the observational error, it is found that a value of *roe* equal to 0.5 dBZ negatively affects the quality of the analyses and of the subsequent forecasts, because the model is not able to remove noise at the smallest scales. This leads to large errors in all prognostic fields in the area where radar data are assimilated and, as a consequence, to a very poor quality of the forecasts. This is particularly significant when 15 minutes assimilation cycles are employed, in which case forecast precipitation is strongly underestimated and mis-located. Conversely, a value of 10 dBZ does not degrade results both in 60

10   minutes and 15 minutes cycles and further tests are necessary to find out if a value grater than 5 dBZ can provide better results. Another improvement of results may be obtained when *roe* is dependent on the range, elevation and radar station, but a better comprehension and estimation of this value is mandatory before testing this configuration.

References

Anderson, J. L.: Spatially and temporally varying adaptive covariance inflation for ensemble filters, Tellus A, 61, 72–83, https://doi.org/10.1111/j.1600-0870.2008.00361.x, http://dx.doi.org/10.1111/j.1600-0870.2008.00361.x, 2009.

Anderson, J. L. and Anderson, S. L.: A Monte Carlo Implementation of the Nonlinear Filtering Problem to Produce Ensemble Assimilations and Forecasts, Monthly Weather Review, 127, 2741–2758, https://doi.org/10.1175/1520-0493(1999)127<2741:AMCIOT>2.0.CO;2, https://doi.org/10.1175/1520-0493(1999)127<2741:AMCIOT>2.0.CO;2, 1999.

Baldauf, M., Seifert, A., Förstner, J., Majewski, D., Raschendorfer, M., and Reinhardt, T.: Operational Convective-Scale Numerical Weather Prediction with the COSMO Model: Description and Sensitivities, Monthly Weather Review, 139, 3887–3905, https://doi.org/10.1175/MWR-D-10-05013.1, https://doi.org/10.1175/MWR-D-10-05013.1, 2011.

Berner, J., Fossell, K. R., Ha, S.-Y., Hacker, J. P., and Snyder, C.: Increasing the Skill of Probabilistic Forecasts: Understanding Performance Improvements from Model-Error Representations, Monthly Weather Review, 143, 1295–1320, https://doi.org/10.1175/MWR-D-14-00091.1, https://doi.org/10.1175/MWR-D-14-00091.1, 2015.

Bick, T., Simmer, C., Trömel, S., Wapler, K., Hendricks Franssen, H.-J., Stephan, K., Blahak, U., Schraff, C., Reich, H., Zeng, Y., and Potthast, R.: Assimilation of 3D radar reflectivities with an ensemble Kalman filter on the convective scale, Quarterly Journal of the Royal Meteorological Society, 142, 1490–1504, https://doi.org/10.1002/qj.2751, http://dx.doi.org/10.1002/qj.2751, 2016.

Bonavita, M., Torrisi, L., and Marcucci, F.: Ensemble data assimilation with the CNMCA regional forecasting system, Quarterly Journal of the Royal Meteorological Society, 136, 132–145, https://doi.org/10.1002/qj.553, http://dx.doi.org/10.1002/qj.553, 2010.

Buehner, M., Houtekamer, P. L., Charette, C., Mitchell, H. L., and He, B.: Intercomparison of Variational Data Assimilation and the Ensemble Kalman Filter for Global Deterministic NWP. Part I: Description and Single-Observation Experiments, Monthly Weather Review, 138, 1550–1566, https://doi.org/10.1175/2009MWR3157.1, https://doi.org/10.1175/2009MWR3157.1, 2010a.

Buehner, M., Houtekamer, P. L., Charette, C., Mitchell, H. L., and He, B.: Intercomparison of Variational Data Assimilation and the Ensemble Kalman Filter for Global Deterministic NWP. Part II: One-Month Experiments with Real Observations, Monthly Weather Review, 138, 1567–1586, https://doi.org/10.1175/2009MWR3158.1, https://doi.org/10.1175/2009MWR3158.1, 2010b.

Clark, P., Roberts, N., Lean, H., Ballard, S. P., and Charlton-Perez, C.: Convection-permitting models: a step-change in rainfall forecasting, Meteorological Applications, 23, 165–181, https://doi.org/10.1002/met.1538, http://dx.doi.org/10.1002/met.1538, mET-14-0154.R1, 2016.

Courtier, P., Andersson, F., Hackley, W., Vasiljevic, D., Hamrud, M., Hollingsworth, A., Rabier, F., Fisher, M., and Pailleux, J.: The ECMWF implementation of three dimensional variational assimilation (3D-Var). I: Formulation, Quarterly Journal of the Royal Meteorological Society, 124, 1783–1807, https://doi.org/10.1002/qj.49712455002, 1998.

Cuo, L., Pagano, T. C., and Wang, Q. J.: A Review of Quantitative Precipitation Forecasts and Their Use in Short- to Medium-Range Streamflow Forecasting, Journal of Hydrometeorology, 12, 713–728, http://www.jstor.org/stable/24912965, 2011.

Davolio, S., Silvestro, F., and Gastaldo, T.: Impact of Rainfall Assimilation on High-Resolution Hydrometeorological Forecasts over Liguria, Italy, Journal of Hydrometeorology, 18, 2659–2680, https://doi.org/10.1175/JHM-D-17-0073.1, https://doi.org/10.1175/JHM-D-17-0073.1, 2017.

Desroziers, G., Berre, L., Chapnik, B., and Poli, P.: Diagnosis of observation, background and analysis-error statistics in observation space, Quarterly Journal of the Royal Meteorological Society, 131, 3385–3396, https://doi.org/10.1256/qj.05.108, http://dx.doi.org/10.1256/qj.05.108, 2005.

Dixon, M., Li, Z., Lean, H., Roberts, N., and Ballard, S.: Impact of Data Assimilation on Forecasting Convection over the United Kingdom Using a High-Resolution Version of the Met Office Unified Model, Monthly Weather Review, 137, 1562–1584, https://doi.org/10.1175/2008MWR2561.1, https://doi.org/10.1175/2008MWR2561.1, 2009.

Doms, G., Förstner, J., Heise, E., Herzog, H.-J., Mironov, D., Raschendorfer, M., Reinhardt, T., Ritter, B., Schrodin, R., Schulz, J.-P., and
5   Vogel, G.: A Description of the Nonhydrostatic Regional COSMO Model, Part II: Physical Parameterization, Tech. rep., http://www.cosmo-model.org/content/model/documentation/core/default.htm, 2011.

Errico, R. M.: Spectra Computed from a Limited Area Grid, Monthly Weather Review, 113, 1554–1562, https://doi.org/10.1175/1520-0493(1985)113<1554:SCFALA>2.0.CO;2, https://doi.org/10.1175/1520-0493(1985)113<1554:SCFALA>2.0.CO;2, 1985.

Evensen, G.: Sequential data assimilation with a nonlinear quasi-geostrophic model using Monte Carlo methods to forecast error statistics,
10   J. Geophys. Res, 99, 10 143–10 162, 1994.

Gustafsson, N. and Bojarova, J.: Four-dimensional ensemble variational (4D-En-Var) data assimilation for the HIgh Resolution Limited Area Model (HIRLAM), Nonlinear Processes in Geophysics, 21, 745–762, https://doi.org/10.5194/npg-21-745-2014, https://www.nonlin-processes-geophys.net/21/745/2014/, 2014.

Hamrud, M., Bonavita, M., and Isaksen, L.: EnKF and Hybrid Gain Ensemble Data Assimilation. Part I: EnKF Implementation, Monthly
15   Weather Review, 143, 4847–4864, https://doi.org/10.1175/MWR-D-14-00333.1, https://doi.org/10.1175/MWR-D-14-00333.1, 2015.

Harnisch, F. and Keil, C.: Initial Conditions for Convective-Scale Ensemble Forecasting Provided by Ensemble Data Assimilation, Monthly Weather Review, 143, 1583–1600, https://doi.org/10.1175/MWR-D-14-00209.1, https://doi.org/10.1175/MWR-D-14-00209.1, 2015.

Houtekamer, P. L. and Mitchell, H. L.: Data Assimilation Using an Ensemble Kalman Filter Technique, Monthly Weather Review, 126, 796–811, https://doi.org/10.1175/1520-0493(1998)126<0796:DAUAEK>2.0.CO;2, https://doi.org/10.1175/1520-0493(1998)126<0796:
20   DAUAEK>2.0.CO;2, 1998.

Houtekamer, P. L. and Mitchell, H. L.: Ensemble Kalman filtering, Quarterly Journal of the Royal Meteorological Society, 131, 3269–3289, https://doi.org/10.1256/qj.05.135, http://dx.doi.org/10.1256/qj.05.135, 2005.

Houtekamer, P. L. and Zhang, F.: Review of the Ensemble Kalman Filter for Atmospheric Data Assimilation, Monthly Weather Review, 144, 4489–4532, https://doi.org/10.1175/MWR-D-15-0440.1, https://doi.org/10.1175/MWR-D-15-0440.1, 2016.

25   Houtekamer, P. L., Mitchell, H. L., Pellerin, G., Buehner, M., Charron, M., Spacek, L., and Hansen, B.: Atmospheric Data Assimilation with an Ensemble Kalman Filter: Results with Real Observations, Monthly Weather Review, 133, 604–620, https://doi.org/10.1175/MWR-2864.1, https://doi.org/10.1175/MWR-2864.1, 2005.

Hunt, B. R., Kostelich, E. J., and Szunyogh, I.: Efficient data assimilation for spatiotemporal chaos: A local ensemble transform Kalman filter, Physica D: Nonlinear Phenomena, 230, 112 – 126, https://doi.org/https://doi.org/10.1016/j.physd.2006.11.008, http://www.sciencedirect.
30   com/science/article/pii/S0167278906004647, data Assimilation, 2007.

Jones, C. D. and Macpherson, B.: A latent heat nudging scheme for the assimilation of precipitation data into an operational mesoscale model, Meteorological Applications, 4, 269–277, https://doi.org/10.1017/S1350482797000522, https://rmets.onlinelibrary.wiley.com/doi/abs/10.1017/S1350482797000522, 2006.

Koinstinen, J. and Puhakka, T.: An improved spatial gauge-radar ad-justment technique, in: Proc. 20th Conference on Radar Meteorology,
35   pp. 179–186, AMS, 1981.

Leuenberger, D. and Rossa, A.: Revisiting the latent heat nudging scheme for the rainfall assimilation in convective system, in: Proc. of 3th European Radar Conference on Radar Meteorology and Hydrology (ERAD), pp. 162–167, Visby, Gotland, Sweden, 6–10 September 2004, 2004.

Leuenberger, D. and Rossa, A.: Revisiting the latent heat nudging scheme for the rainfall assimilation of a simulated convective storm, Meteorol. Atmos. Phys., 98, 195–215, 2007.

Lin, Y.-L., Farley, R. D., and Orville, H. D.: Bulk Parameterization of the Snow Field in a Cloud Model, Journal of Climate and Applied Meteorology, 22, 1065–1092, https://doi.org/10.1175/1520-0450(1983)022<1065:BPOTSF>2.0.CO;2, https://doi.org/10.1175/1520-0450(1983)022<1065:BPOTSF>2.0.CO;2, 1983.

Meng, Z. and Zhang, F.: Limited-Area Ensemble-Based Data Assimilation, Monthly Weather Review, 139, 2025–2045, https://doi.org/10.1175/2011MWR3418.1, https://doi.org/10.1175/2011MWR3418.1, 2011.

Mitchell, H. L. and Houtekamer, P. L.: An Adaptive Ensemble Kalman Filter, Monthly Weather Review, 128, 416–433, https://doi.org/10.1175/1520-0493(2000)128<0416:AAEKF>2.0.CO;2, https://journals.ametsoc.org/doi/abs/10.1175/1520-0493%282000%29128%3C0416%3AAAEKF%3E2.0.CO%3B2, 2000.

Miyoshi, T., Sato, Y., and Kadowaki, T.: Ensemble Kalman Filter and 4D-Var Intercomparison with the Japanese Operational Global Analysis and Prediction System, Monthly Weather Review, 138, 2846–2866, https://doi.org/10.1175/2010MWR3209.1, https://doi.org/10.1175/2010MWR3209.1, 2010.

Nastrom, G. D. and Gage, K. S.: A Climatology of Atmospheric Wavenumber Spectra of Wind and Temperature Observed by Commercial Aircraft, Journal of the Atmospheric Sciences, 42, 950–960, https://doi.org/10.1175/1520-0469(1985)042<0950:ACOAWS>2.0.CO;2, https://doi.org/10.1175/1520-0469(1985)042<0950:ACOAWS>2.0.CO;2, 1985.

Raschendorfer, M.: The new turbulence parametrization of LM, COSMO newsletter, 1, 89–97, 2001.

Ritter, B. and Geleyn, J.-F.: A Comprehensive Radiation Scheme for Numerical Weather Prediction Models with Potential Applications in Climate Simulations, Monthly Weather Review, 120, 303–325, https://doi.org/10.1175/1520-0493(1992)120<0303:ACRSFN>2.0.CO;2, https://doi.org/10.1175/1520-0493(1992)120<0303:ACRSFN>2.0.CO;2, 1992.

Röpnack, A., Hense, A., Gebhardt, C., and Majewski, D.: Bayesian Model Verification of NWP Ensemble Forecasts, Monthly Weather Review, 141, 375–387, https://doi.org/10.1175/MWR-D-11-00350.1, https://doi.org/10.1175/MWR-D-11-00350.1, 2013.

Rossa, A., Nurmi, P., and Ebert, E.: Overview of methods for the verification of quantitative precipitation forecasts, pp. 419–452, Springer Berlin Heidelberg, Berlin, Heidelberg, https://doi.org/10.1007/978-3-540-77655-0_16, https://doi.org/10.1007/978-3-540-77655-0_16, 2008.

Schraff, C., Reich, H., Rhodin, A., Schomburg, A., Stephan, K., Periáñez, A., and Potthast, R.: Kilometre-scale ensemble data assimilation for the COSMO model (KENDA), Quarterly Journal of the Royal Meteorological Society, 142, 1453–1472, https://doi.org/10.1002/qj.2748, http://dx.doi.org/10.1002/qj.2748, 2016.

Seifert, A. and Beheng, K. D.: A double-moment parameterization for simulating autoconversion, accretion and selfcollection, Atmospheric Research, 59-60, 265 – 281, https://doi.org/https://doi.org/10.1016/S0169-8095(01)00126-0, http://www.sciencedirect.com/science/article/pii/S0169809501001260, 13th International Conference on Clouds and Precipitation, 2001.

Skamarock, W. C.: Evaluating Mesoscale NWP Models Using Kinetic Energy Spectra, Monthly Weather Review, 132, 3019–3032, https://doi.org/10.1175/MWR2830.1, https://doi.org/10.1175/MWR2830.1, 2004.

Sokol, Z.: Effects of an assimilation of radar and satellite data on a very-short range forecast of heavy convective rainfalls, Atmospheric Research, 93, 188 – 206, https://doi.org/https://doi.org/10.1016/j.atmosres.2008.11.001, http://www.sciencedirect.com/science/article/pii/S0169809508003402, 4th European Conference on Severe Storms, 2009.

Stephan, K., Klink, S., and Schraff, C.: Assimilation of radar-derived rain rates into the convective-scale model COSMO-DE at DWD, Quarterly Journal of the Royal Meteorological Society, 134, 1315–1326, https://doi.org/10.1002/qj.269, http://dx.doi.org/10.1002/qj.269, 2008.

Tiedtke, M.: A Comprehensive Mass Flux Scheme for Cumulus Parameterization in Large-Scale Models, Monthly Weather Review,
5 117, 1779–1800, https://doi.org/10.1175/1520-0493(1989)117<1779:ACMFSF>2.0.CO;2, https://doi.org/10.1175/1520-0493(1989)117<1779:ACMFSF>2.0.CO;2, 1989.

Tong, M. and Xue, M.: Ensemble Kalman Filter Assimilation of Doppler Radar Data with a Compressible Nonhydrostatic Model: OSS Experiments, Monthly Weather Review, 133, 1789–1807, https://doi.org/10.1175/MWR2898.1, https://doi.org/10.1175/MWR2898.1, 2005.

Wang, X., Barker, D. M., Snyder, C., and Hamill, T. M.: A Hybrid ETKF–3DVAR Data Assimilation Scheme for the WRF Model. Part I:
10 Observing System Simulation Experiment, Monthly Weather Review, 136, 5116–5131, https://doi.org/10.1175/2008MWR2444.1, https://doi.org/10.1175/2008MWR2444.1, 2008.

Wernli, H., Paulat, M., Hagen, M., and Frei, C.: SAL—A Novel Quality Measure for the Verification of Quantitative Precipitation Forecasts, Monthly Weather Review, 136, 4470–4487, https://doi.org/10.1175/2008MWR2415.1, https://doi.org/10.1175/2008MWR2415.1, 2008.

Wernli, H., Hofmann, C., and Zimmer, M.: Spatial Forecast Verification Methods Intercomparison Project: Application of the SAL Technique,
15 Weather and Forecasting, 24, 1472–1484, https://doi.org/10.1175/2009WAF2222271.1, https://doi.org/10.1175/2009WAF2222271.1, 2009.

Zängl, G., Reinert, D., Rípodas, P., and Baldauf, M.: The ICON (ICOsahedral Non-hydrostatic) modelling framework of DWD and MPI-M: Description of the non-hydrostatic dynamical core, Quarterly Journal of the Royal Meteorological Society, 141, 563–579, https://doi.org/10.1002/qj.2378, http://dx.doi.org/10.1002/qj.2378, 2015.

20 Zhang, F., Snyder, C., and Sun, J.: Impacts of Initial Estimate and Observation Availability on Convective-Scale Data Assimilation with an Ensemble Kalman Filter, Monthly Weather Review, 132, 1238–1253, https://doi.org/10.1175/1520-0493(2004)132<1238:IOIEAO>2.0.CO;2, https://doi.org/10.1175/1520-0493(2004)132<1238:IOIEAO>2.0.CO;2, 2004.